RSC Advances

ROYAL SOCIETY OF CHEMISTRY

www.rsc.org/advances

Cite this: DOI: 10.1039/c0xx00000x

www.rsc.org/xxxxxx

ARTICLE TYPE

Li_2FePO_4F and its metal-doping for Li-ion batteries: An *ab initio* study

Fengmei Yang,[a] Weiwei Sun,[b] Yuhan Li,[a] Haiyan Yuan,[a] Zhiyong Dong,[a] Huanhuan Li,[a] Jumei Tian,[a] Yiying Zheng,*[a] Jingping Zhang*[a]

Received (in XXX, XXX) Xth XXXXXXXXX 20XX, Accepted Xth XXXXXXXXX 20XX
DOI: 10.1039/b000000x

The electrochemical properties of three isotopic Li_2FePO_4F compounds, as cathode materials under different space groups *Pbcn*, *P$\bar{1}$* and *Pnma* were investigated using first principle calculations. Their structures, average open circuit voltages for step delithiation reactions were explored, the results are in good agreement with the reported experimental data. We estimate the substitution effect of Fe by Co in *Pnma*-Li_2FePO_4F. The substitution of Fe by Co in $Li_2Fe_{1-x}Co_xPO_4F$ may enhance the discharge potential of the materials, and the rate of its volume change during the redox process is between 0.6% ~ 2.1%. Furthermore, from the projected density of states for $Li_2Fe_{0.5}Co_{0.5}PO_4F$, we found a strong hybridization for Fe-3*d*, Co-3*d* bands near the Fermi level, which implies that the Co-doped $Li_2Fe_{1-x}Co_xPO_4F$ may possess better electronic conductivity than the pure phase.

1 Introduction

Commercialized lithium ion battery (LIB) has rapidly penetrated into everyday life since Sony announced the first version in 1992.[1-6] Important battery performance characteristics are mainly determined by the electrochemical properties of the electrode materials, especially the cathode. The conventional positive materials for LIB such as $LiCoO_2$, Li_2MnO_3 and $LiFePO_4$ have been widely studied and optimized.[7, 8] For example, $LiFePO_4$ is the most prominent compound in the transition metal polyanionic family,[9, 10] and its major limitations are the poor electrical conductivity and the one-dimensional Li-ion diffusion. Its relatively poor electronic conductivity can be more than offset by decreasing the size of crystallite[11], doping transition metal[12] and coating conductive additives onto the surface[13]. However these strategies increased the complexity and reduced the reliability of the material's manufacture, hence it is desirable to develop new polyanion-type cathode materials for lithium ion batteries. Yang *et al* had reported a detailed description for this families,[14] one of the most interesting poly-anion compounds is that of fluorophosphates. A_2MPO_4F materials (A = Na, Li; M = Fe, Mn, Co, Ni, etc.) have been proposed as promising candidates for high-energy-cathode materials, especially for A = Li.[15-23]

The Li_2MPO_4F family has attracted much attention for the following reasons: firstly, fluorophosphates compounds exhibit high specific capacity and energy density, when the exchange of more than one alkali atom per formula unit (*f.u.*) was considered. Secondly, it possesses facile two-dimensional pathways for Li^+ transportation and the structure changes on redox are relatively small.[17 20] Additionally, the high electronegativity of F^- serves to increase the thermal stability of Li_2MPO_4F compared to $LiMPO_4$.[17] Four space groups for Li_2MPO_4F have been widely investigated experimentally: *Pnma* (M = Fe, Ni, Co)[18, 19, 21], *Pbcn* (M = Fe)[17], *P$\bar{1}$* (M = Fe)[20, 24], *P2$_1$/n* (M = Mn).[16, 22] Accordingly, Li_2FePO_4F could adopt both tetragonal and triclinic structures, which depends on synthetic procedures.[17, 20-22] The synthesis of Li_2FePO_4F remains difficult and requires either the ion exchange of the Na_2FePO_4F/$LiNaFePO_4F$ or a lengthy solid state reaction.[17, 20, 21] One appealing strategy for improving the cathode properties is to develop mixed transition metal compounds,[25-28] this approach has been widely applied to other material families. The influence of metal-doping on the performance of a cathode material for LIB has been investigated from both theoretical and experimental aspects.[12, 29-31] Nevertheless, to the best of our knowledge, the metal-doping for Li_2FePO_4F has not yet been reported. High-throughput density functional theory calculations had been explored and made enormous contribution to the LIB field in predicting the structural behavior and electrochemical properties. To individuate the most promising candidates for practical applications and optimize *Pnma*-Li_2FePO_4F, we investigated the electrochemical and electronic properties by metal-doping (M = Co) using *ab initio* methods.

Herein we systematically investigated the influence of crystal structure and relative stability on the electrochemical properties of Li_2FePO_4F polymorphs as cathode materials for LIB. A comparative study of three reported polymorphs crystallized of Li_2FePO_4F (with space groups *Pbcn*, *P$\bar{1}$*, *Pnma*) was also performed. Our computed structures, average open circuit voltages of Li_2FePO_4F are in good agreement with the experimental data. The calculated results revealed that *Pnma*-Li_2FePO_4F possesses the highest electron conductivity among investigated space groups. We explored the structure, electrochemical stability and projected density of states (PDOS) of substitution of Fe by various degree levels of Co using first principle computations as a screening tool.

2 Computational methods

All the calculations were performed by using *ab inito* methods implemented in the Vienna *Ab Initio* simulation package (VASP),[32-35] which is based on the density functional theory (DFT). Generalized-gradient approximation (GGA) with the

functional of Perdew, Burke and Ernzerhof (PBE) was used to describe the potential. Projector augmented wave (PAW) was employed to describe the electron wave functions.[36] PAW method has been widely used for battery materials and shown excellent predictive capability.[37-39] The *GGA+U* method was used to accurately calculate structural and electronic properties, because of the strong localization of the 3*d* orbital such as phosphate materials, incomplete cancellation of the self-interaction of the *GGA* is often reported to cause large errors.[40] We used the effective U parameter for transition metals (TM), U_{Fe} = 4.5 eV[41], U_{Mn} = 4.5 eV[41], and U_{Co} = 3.4 eV[42], respectively. A planewave cutoff energy of 400 eV was used for all computations, and appropriate *k*-points meshes were chosen to ensure that the total energies were converged within 2 meV per *f.u*. Gaussian smearing was used with a smearing parameter of 0.20 eV. The calculated energy difference between ferromagnetic (FM) and antiferromagnetic (AFM) ordering was less than 6.5 meV per *f.u*, implying that the magnetic structure has less effect on the energy calculations. Thus the calculations were performed in a high-spin ferromagnetic ordering. Initial magnetic moments were set to high-spin for Mn, Fe, and Co and low-spin for other elements.[43]

The initial atomic positions for Li_2FePO_4F were taken from Ref 20 ($P\bar{1}$), Ref 17 (*Pbcn*), Ref 21 (*Pnma*), and the two Li ions were removed from the Li_2FePO_4F polymorphs to generate $FePO_4F$. For the intermediate $LiFePO_4F$, the Li-vacancy arrangements were taken from the Refs 17, 21 and 20 for *Pbcn*, *Pnma* and $P\bar{1}$, respectively. For metal-doping calculations, all structures were fully relaxed (cell parameters, cell volume, and atomic positions), and performed in an 8-*f.u*. Li_2FePO_4F supercell, in which 1-8 Fe atoms were replaced one by one by Co atom, respectively. The migration energy barriers for diffusion of Li atom are calculated by the Cl-NEB method[44].

Ab initio methods have been widely used to predict the average voltages of lithium deintercalation/intercalation in many compounds.[45, 46] Following the well-established methods, the open circuit voltage (OCV) V *vs*. Li/Li$^+$ can be calculated from the energy difference, if volume and entropy effects are neglected[7]:

$$\mathrm{OCV}(x,y)(y>x) = -\frac{[\mathrm{Etol}(\mathrm{LiyFePO_4F}) - \mathrm{Etol}(\mathrm{LixFePO_4F}) - (y-x)\mathrm{Etol}(\mathrm{Li})]}{(y-x)}$$

3 Results and discussion

3.1 Cell parameters, energy and structural characteristics of Li_2FePO_4F polymorphs

In this work, three Li_2FePO_4F polymorphs with the space groups of *Pbcn*, $P\bar{1}$ and *Pnma* are considered. Their optimized lattice parameters, volumes changes and average voltages are listed in Table 1, together with the available experimental results. For the three polymorphs of Li_2FePO_4F, the calculated lattice parameters are in good accordance with the experimental data, for example, the discrepancies between calculated and experimental volumes of the unit cell are lower than 2.55%. Noting that our calculated results for *Pbcn*-Li_2FePO_4F polymorph are consistent with the previous report.[47]

We also compared the electrochemical properties of three compounds, the average deintercalation voltage for the first and second Li$^+$ are show in Table 1. In $P\bar{1}$-Li_2FePO_4F, $Fe^{3+}\rightarrow Fe^{2+}$ redox couple is at 2.7 V *vs* Li/Li$^+$, about 0.7 V lower than the same redox transition in *Pbcn*-Li_2FePO_4F and *Pnma*-Li_2FePO_4F. For all the polymorphs, the oxidation of Fe^{3+} to Fe^{4+} occurs at a very high voltage (~5.1 V), which makes it necessary to use an electrolyte with a wide electrochemical window, like ionic liquids. Fig. 1 shows the calculated total energy as a function of volume obtained from the Li_yFePO_4F (y =2, 1, 0). For Li_2FePO_4F, the total energy differences between *Pbcn* and *Pnma*-Li_2FePO_4F polymorphs are very small at 0 K, this phenomenon explains why synthesis of Li_2FePO_4F need to use ion exchange of the Na-counterparts[17, 21], while for synthesized directly may easily result in a mixture of *Pbcn* and *Pnma*-Li_2FePO_4F. And the total energy of *Pbcn* and *Pnma*-Li_2FePO_4F is lower than $P\bar{1}$-Li_2FePO_4F, hence $P\bar{1}$-Li_2FePO_4F was less stable than *Pbcn* and *Pnma*. We stress that tavorite-type structure of $P\bar{1}$-Li_2FePO_4F prepared by reduction of $LiFePO_4F$ differs greatly from ion-exchange of the Na-counterparts[20].

From Fig. 1, it can be observed that the unit cell volume contracts during the first and second delithiation step for both $P\bar{1}$ and *Pnma*-Li_2FePO_4F, however the unit cell volume increases for *Pbcn*-Li_2FePO_4F when it is fully delithiated to form $FePO_4F$, this phenomena is correlated with *d-p* mixing.[41]

In Fig. 2, all Li_2FePO_4F polymorphs are built of FeO_4F_2 octahedra and PO_4 tetrahedra, and each Fe atom is surrounded by two fluorine atoms and four oxygen atoms. The connectivity of the octahedral varies from the layered structure to the 3D structure.

Table 1 The optimized lattice parameters, specific capacities, volume changes, and average voltages for Li_2FePO_4F of *Pbcn*, $P\bar{1}$, and *Pnma* space groups, compared with available results

Li_2FePO_4F	*Pbcn*			$P\bar{1}$		*Pnma*	
lattice parameter	Calc	Exp[a]	Ref[b]	Calc	Exp[c]	Calc	Exp[d]
a(Å)	4.99	5.05	4.95	5.34	5.37	10.61	10.78
b(Å)	13.07	13.56	13.09	7.35	7.48	6.33	6.27
c(Å)	11.37	11.05	11.17	5.35	5.33	11.13	11.03
V(Å^3)	742.06	723.60	757.62	184.64	189.14	746.8	744.5
Volume Discrepancies	2.55 %			2.34 %		0.31%	
Fe^{3+}/Fe^{2+} (V)	3.27	3.50		2.43	2.75	3.50	3.40
Fe^{4+}/Fe^{3+} (V)	5.20			5.09		5.02	

[a-d] From Ref 17, 46, 20, 21, respectively

Figs. 2a and 2b show the orthorhombic structure of *Pbcn*-Li_2FePO_4F with the layered structural features including pairs of

face-sharing metal octahedra, two alkali-ions locate in the interlayer space, and two-dimensional pathways for Li^+ transport[17]. In the triclinic $P\bar{1}$ tavorite-type framework (Fig. 2c), the FeF_2O_4 octahedra forms corner-sharing 1D chain in the *b* axis with alternating tilted octahedral bridged by the F^- ions, and these chains are connected by corner-sharing the phosphate tetrahedra to create a spacious 3D structure. For the *Pnma*-Li_2FePO_4F (Figs. 2d, 2e and 2f), the structure consists of edge-sharing chains of FeF_2O_4 octahedra running along the *b* axis, and the channels along the [011] and [010] are capable of Li^+ diffusion.

Nellie *et al* also showed experimentally that the *Pnma*-Li_2FePO_4F with a 3D framework exhibits several advantages over other iron-based fluorophosphates, for instance, the volume change upon redox is one quarter of $P\bar{1}$-Li_2FePO_4F and a half of *Pbcn*-Li_2FePO_4F.[21]

3.2 Factor-Q for three Li_2FePO_4F polymorphs

The search for a general quality criterion addressing the potential of three polymorphs of Li_2FePO_4F as cathode materials should be taken fully into account both the OCV and band gaps (BG) values. A material with a high electrochemical potential which make it an attractive candidate for cathodes used in high-energy batteries. The high OCV corresponds to a high electrochemical potential, while the low BG corresponds to high electronic conductivity of material. Mustarelli *et al* raise the Quality factor, Q,[25] which is proposed by combining the above-mentioned observables:

$$Q = OCV / BG$$

We calculated total density of states of Li_2FePO_4F/$LiFePO_4F$ (see ESI† Fig. S1), the BG are determined from the calculated density of states and listed in Table 2. It is shown that both Li_2FePO_4F and $LiFePO_4F$, the lowest BG values are obtained in the frame of the *Pnma* space group.

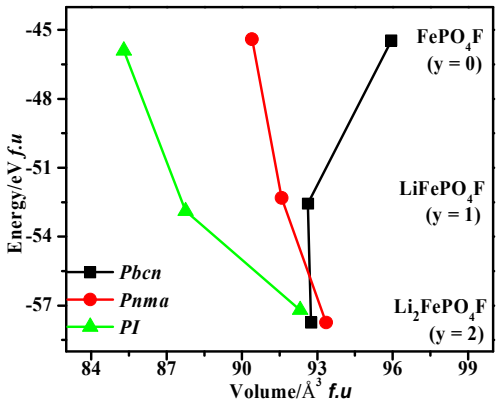

Fig. 1 Calculated total energy *vs* volume curves for *Pbcn*, $P\bar{1}$ and *Pnma* polymorphs of Li_yFePO_4F (y =2, 1, 0).

The calculated behaviors of the Q for Li_2FePO_4F and $LiFePO_4F$ with three space groups are presented in Fig. 3. Q values were increased from lithiated states (Purple) to delithiated (Dark yellow) states of $LiFePO_4F$. Compared with *Pbcn* and $P\bar{1}$ Li_2FePO_4F/$LiFePO_4F$ polymorphs, *Pnma*-Li_2FePO_4F/$LiFePO_4F$ may be the best cathode material with the largest Q values.

Table 2 The values of band gaps for Li_2FePO_4F and $LiFePO_4F$ with three space groups

Space group	BG (Li_2FePO_4F)/eV	BG ($LiFePO_4F$)/eV
Pnma	3.196	1.301
Pbcn	3.465	2.578
$P\bar{1}$	3.639	2.539

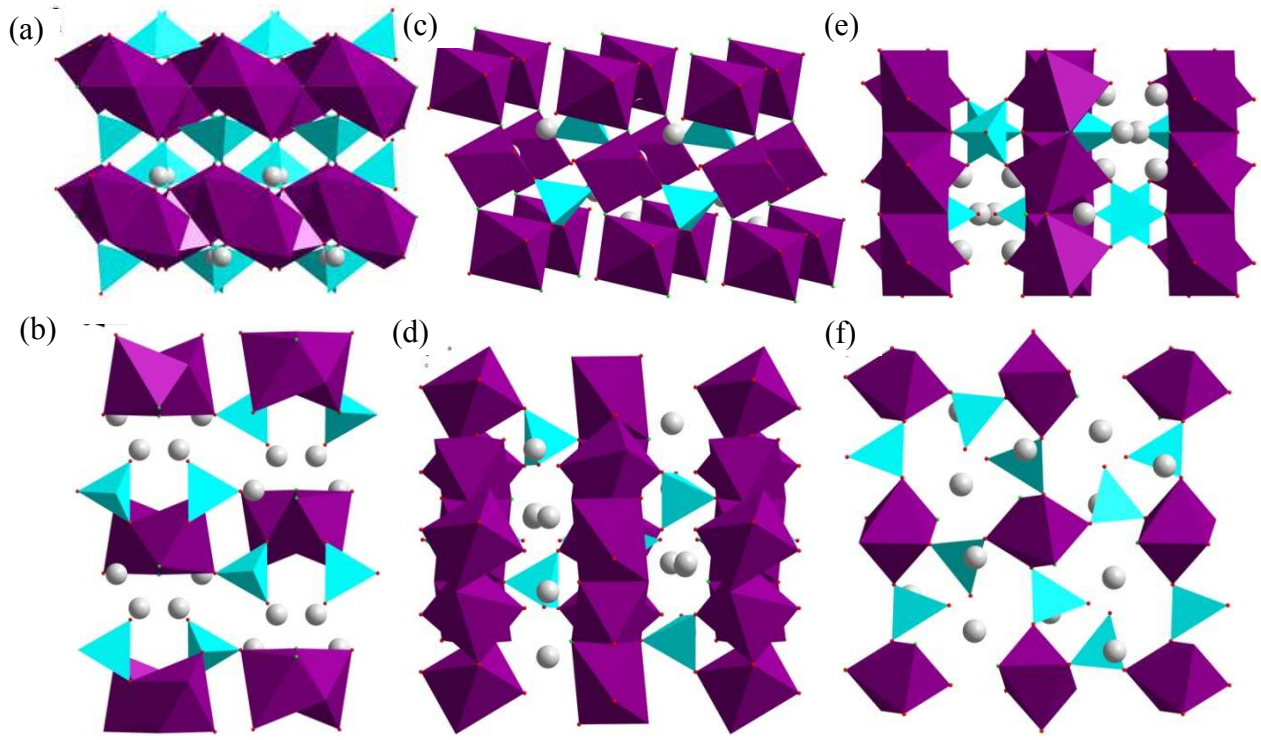

Fig. 2 The optimized crystal structures of three Li_2FePO_4F polymorphs. *Pbcn*: ((a) and (b)) view along the *b* and *c* axis, respectively; $P\bar{1}$: (c) view along the *c* axis; *Pnma*: (d), (e), and (f) represent the direction of [100], [011], [010], respectively. Violet octahedra, turquoise tetrahedra, and gray balls represent FeO_4F_2, PO_4 and Li^+, respectively.

Cite this: DOI: 10.1039/c0xx00000x

www.rsc.org/xxxxxx

ARTICLE TYPE

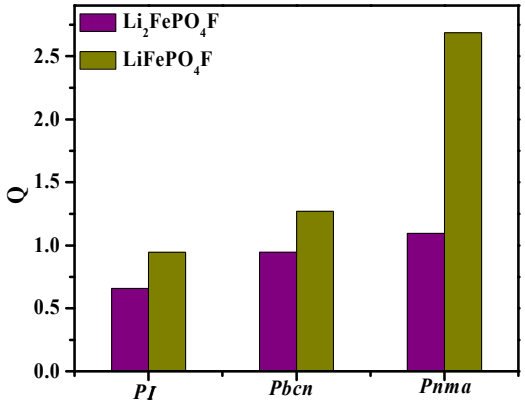

Fig. 3 The behaviors of the Q for Li_2FePO_4F and $LiFePO_4F$ with three space groups.

3.3 Co−doped *Pnma*-Li_2FePO_4F

It is well known that the Co^{2+}/Co^{3+} has a relatively high redox voltage. For example, fluoride phosphate Li_2CoPO_4F[19, 48, 49] possesses the highest redox potential among available cathodes currently (5.1 V vs. Li/Li^+). It can be expected that the substitution of Co for Fe at $Li_2Fe_{1-x}Co_xPO_4F$ (x = 1/8, 2/8, 3/8, 4/8, 5/8, 6/8, 7/8,1) may increase the discharge potential (*i.e.* energy density) of the materials. Moreover, *Pnma*-Li_2CoPO_4F is isostructural with *Pnma*-Li_2FePO_4F, hence Co-doped *Pnma*-Li_2FePO_4F, *i.e.* $Li_2Fe_{1-x}Co_xPO_4F$ (x = 1/8, 2/8, 3/8, 4/8, 5/8, 6/8, 7/8,1), may not occur a phase transformation like $Na_2Fe_{1-x}Mn_xPO_4F$[50]. Previous report revealed that the Li_2MnPO_4F belongs to the $P2_1/n$ space group[16], for comparison, we investigate the stability of the Co/Mn−doped *Pnma*-Li_2FePO_4F as well (see detail in the ESI†). The calculated results suggest that $Li_2Fe_{1-x}Co_xPO_4F$ (x = 1/8, 2/8, 3/8, 4/8, 5/8, 6/8, 7/8,1) is stable enough as a new cathode material, but $Li_2Fe_{1-x}Mn_xPO_4F$ (x = 1/8, 2/8, 3/8, 4/8, 5/8, 6/8, 7/8,1) might easily decomposed into $LiMnPO_4$, $LiFePO_4$ and LiF (as illustrated in Fig. S2 in ESI†). This can be traced back to the isostructural of Li_2CoPO_4F with *Pnma*-Li_2FePO_4F, while Li_2MnPO_4F is different. Hereafter, we estimate the structure, electrochemical properties and PDOS of $Li_2Fe_{1-x}Co_xPO_4F$ (x = 1/8, 2/8, 3/8, 4/8, 5/8, 6/8, 7/8,1) in the following calculations.

3.3.1 The lattice parameters of $Li_2Fe_{1-x}Co_xPO_4F$ (x = 1/8, 2/8, 3/8, 4/8, 5/8, 6/8, 7/8)

The lattice parameters and unit cell volume for $Li_2Fe_{1-x}Co_xPO_4F$ (0 < x < 1) are summarized in Fig. 4. The *a* and *b* lattice parameters almost remain the same upon the substitution of Fe by Co, while *c* values are decreased. As a result, the unit cell volume of $Li_2Fe_{1-x}Co_xPO_4F$ should decrease with the substitution of Co for Fe, because of the ionic radius $Fe^{II} > Co^{II}$ (Co^{II}: 0.745 Å, Fe^{II}: 0.780 Å for high-spin state within six-fold coordination)[51]. To evaluate the affect of decrease volume to the Li conductivity in the materials, we also calculated the activation barriers of $Li_2Fe_{1-x}Co_xPO_4F$ (x = 0. 0.25, 0.75) in the ESI† (Fig. S5). It is found that the higher doping concentration leads to higher migration barriers for diffusion of Li.

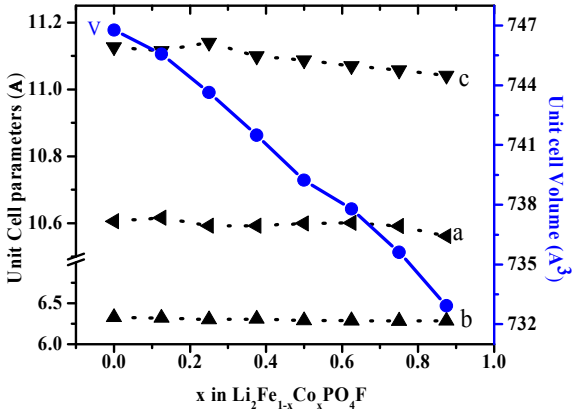

Fig. 4 The unit cell parameters and volumes for different compounds of $Li_2Fe_{1-x}Co_xPO_4F$ (x = 1/8, 2/8, 3/8, 4/8, 5/8, 6/8, 7/8).

3.3.2 Most probable doping model

There are two distinct positions for Fe, namely $Fe_{(1)}$ (4a sites) and $Fe_{(2)}$ (4b sites) in *Pnma*-Li_2FePO_4F structure though they have same coordination environments (ESI†, Fig.S3). From Table 3, it is clear that the Fe-X distances and the O-Fe-O/F angles are different for $Fe_{(1)}O_4F_2$ and $Fe_{(2)}O_4F_2$ octahedra. The distance of $Fe_{(1)}$-O (2.08 Å) and $Fe_{(2)}$-O (2.05 Å) are similar, while the average bond length of $Fe_{(2)}$-F is ~0. 1 Å longer than that of $Fe_{(1)}$-F. The increasing of Fe-F distance may cause the decrement of static electricity, and Co may be inclined to substitute for $Fe_{(2)}$ (4b sites) atom. *Pnma*-Li_2FePO_4F has some distortion in the $Fe_{(1)}O_4F_2$ and $Fe_{(2)}O_4F_2$ octahedra, which may reduce the structural stability. For instant, the higher distortion of angles of O-$Fe_{(1)}$-O/F than those of O-$Fe_{(2)}$-O/F may results in the higher instability of $Fe_{(1)}O_4F_2$ octahedra structure.

We calculated the energies of 23 configurations for $Li_2Fe_{1-x}Co_xPO_4F$ (x = 1/8, 2/8, 3/8, 4/8, 5/8, 6/8, 7/8, 1), in the *Pnma* host, using the supercells up to 8-*f.u* ($Li_{16}Fe_8P_8O_{32}F_8$). In Fig.5, we displayed the total energies (in black) and unit cell volume (in red) for most stable substituted $Li_2Fe_{1-x}Co_xPO_4F$ (0 < x < 1), where the labels (1) and (2) refer to positions of Fe.

Table 3 Optimized Fe-O/F average lengths and angles of O-Fe-O/F

Bonds	Average Length (Å)	Angle	Value (°)
$Fe_{(1)}$-O	2.08	O-$Fe_{(1)}$-O	84.99
$Fe_{(2)}$-O	2.05	O-$Fe_{(2)}$-O	85.61
$Fe_{(1)}$-F	2.13	O-$Fe_{(1)}$-F	101.42
$Fe_{(2)}$-F	2.22	O-$Fe_{(2)}$-F	97.94

From Fig. 5, it is evident that the substitution of Co for $Fe_{(2)}$ at $Li_2Fe_{1-x}Co_xPO_4F$ possesses lower energy values than $Fe_{(1)}$. Consequently, $Fe_{(2)}$ may be more favorable in the Co substitution than $Fe_{(1)}$. When x = 0.375, the energy for 222 site is only 0.85 meV/*f.u* higher than that of 221 site, nevertheless, such a small value is at the range of error limitation. For the different concentrations of 12.5%, 25%, 37.5%, the trend is that the most

Cite this: DOI: 10.1039/c0xx00000x

www.rsc.org/xxxxxx

ARTICLE TYPE

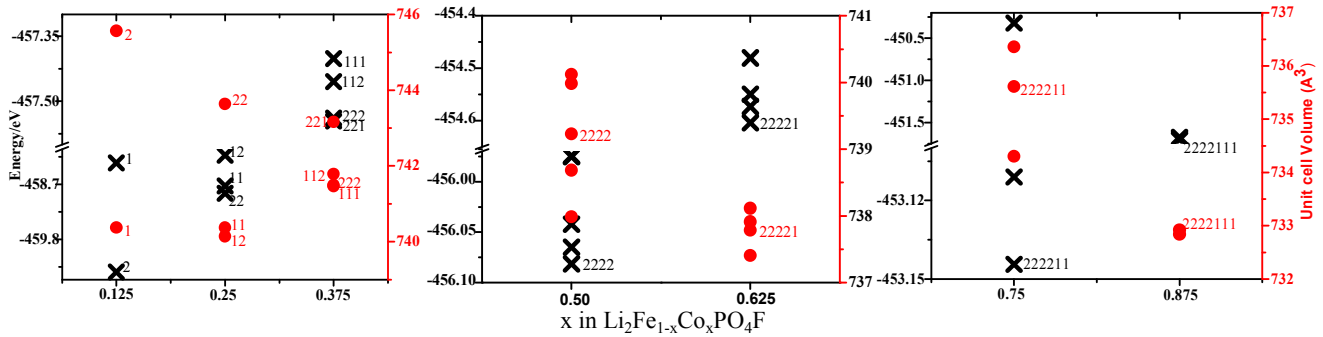

Fig. 5 The calculated energies and unit cell volume for $Li_2Fe_{1-x}Co_xPO_4F$ (x = 1/8, 2/8, 3/8, 4/8, 5/8, 6/8, 7/8).

stable multicomponent fluorophosphates compounds (with lower total energy) have the largest volume. However, no direct correlation between the volume and the total energy were observed at other concentrations. We also calculated the energies of vacancies of $Fe_{(1)}$ and $Fe_{(2)}$, and the results show that $Fe_{(2)}$ vacancy has lower total energy, consequently, Co may substitute the Fe atom at the $Fe_{(2)}$ site preferentially.

3.3.3 OCV

It is instructive to investigate the electrochemical parameter OCV, which usually contains enough information to decide whether a material is of interest as a cathode candidate for Li-ion batteries.[41] Fig. 6 shows the two voltages corresponding to the extraction of two Li ions in two consecutive electron redox processes. These results also confirmed our former prediction that the substitution of Co for Fe at $Li_2Fe_{1-x}Co_xPO_4F$ (x = 1/8, 2/8, 3/8, 4/8, 5/8, 6/8, 7/8) can increase the discharge potential of the material. Interestingly, the first voltage step (y from 2 to 1) increases 0.1 V, when the concentration of Co increases by 12.5%, while the fully delithiated voltage step (y from 1 to 0) increases by about 0.02 V with the substitution of Co for Fe. The volume changes of $Li_2Fe_{1-x}Co_xPO_4F$ (x = 1/8, 2/8, 3/8, 4/8, 5/8, 6/8, 7/8) upon redox are in the range of 0.6%~2.1% (see ESI†, Fig. S4), which is smaller than that of $LiFePO_4$ (6.7%), indicating that $Li_2Fe_{1-x}Co_xPO_4F$ is stable enough to be new cathode materials.

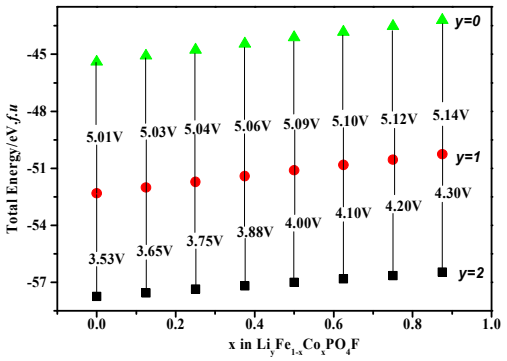

Fig. 6: The calculated total energy for $Li_yFe_{1-x}Co_xPO_4F$ in the lithiated (y=2), semi-delithiated phase (y=1) and full-delithiated phase (y=0) together with the calculated cell voltages.

3.3.4 Electronic structure of $Li_2Fe_{1-x}Co_xPO_4F$

To evaluate the electron properties we calculated the electronic structure of $Li_2Fe_{1-x}Co_xPO_4F$. Fig. 7 shows the PDOS onto the *d*-orbital of the TM of the $Li_2Fe_{1-x}Co_xPO_4F$ (x = 0.25, 0.375, 0.5, 0.75). Only electron states near the Fermi level play the key role in the electron transport processes, thus we mainly focus on the PDOS around the Fermi energy. Careful inspection of Fig. 7 demonstrates that there are two parts in the DOS patterns around the Fermi level those are un-completely filled 3*d* orbitals of transition metal located below the Fermi level, and empty 3*d* orbitals located above the Fermi level.[25] For $Li_2Fe_{0.75}Co_{0.25}PO_4F$ that is x = 0.25 both valence and conduction states are mainly contributed from Fe 3*d* orbitals. When x = 0.375 the conduction bands localized about 3.0 eV are mainly due to Co-3*d* states and this configuration leads to a lower BG, while for x = 0.75, the energy region just above Fermi level dominated by unoccupied Co 3*d* orbitals. It is interesting to note that at the concentration of 50%, *i.e.* $Li_2Fe_{0.5}Co_{0.5}PO_4F$, the occupied Co-3*d* states are strongly hybridized with the Fe-3*d* states near the Fermi level. The $Li_2Fe_{1-x}Co_xPO_4F$ can be considered as semiconductor at the Co concentration of x= 0.25, 0.375, and 0.75; while this material shows metallic at x=0.5. To investigate the difference electronic properties of $Li_2Fe_{1-x}Co_xPO_4F$ (x = 0.25, 0.5, 0.75), we plotted the electron localization function (ELF) in the ESI† (see Fig. S6). Thereby with the increasing of Co doping content, the contribution of 3*d* orbital of cobalt to the TDOS around the Fermi level is increases correspondingly. Thus, the Co-doped Li_2FePO_4F may have better electronic conductivity than the pure phase.

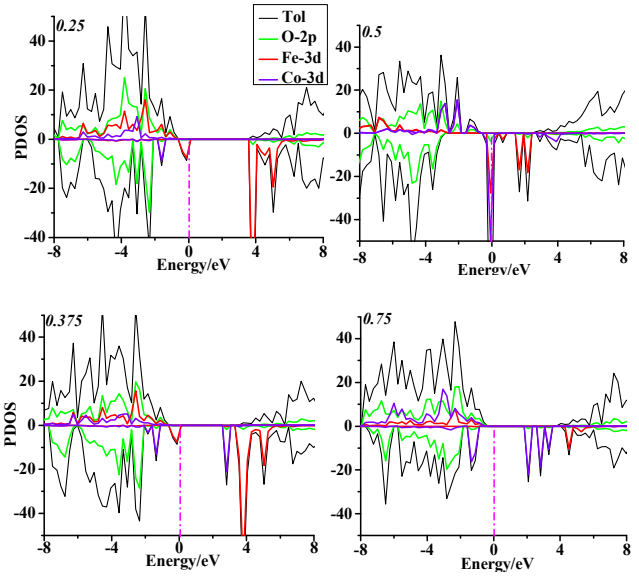

Fig. 7 The calculated PDOS of $Li_2Fe_{1-x}Co_xPO_4F$ (x = 0.25, 0.375, 0.5, 0.75), PDOS for different atoms are denoted by different colors to indicate their contribution.

4 Conclusion

We have investigated the *Pbcn*, *PĪ* and *Pnma* space groups of Li_2FePO_4F by using first-principle DFT computations. The calculated average intercalation voltages, as well as the lattice parameters, agree well with available experimental results. In particular, *Pnma*-Li_2FePO_4F is interesting as far as the electron conductivity is concerned. For transition metal doped *Pnma*-Li_2FePO_4F, $Li_2Fe_{1-x}Co_xPO_4F$ may be stable enough to be used as new cathode materials. Furthermore, the substitution of Co for Fe *i.e.* $Li_2Fe_{1-x}Co_xPO_4F$ ($0 < x < 1$) favors to increase the discharge potential of the pure materials, although the migration barriers for diffusion of Li are increased to some extent as well. The small volume change (0.6% ~ 2.1%) on the removal of one or two Li^+ per *f.u*, suggests that $Li_2Fe_{1-x}Co_xPO_4F$ (x = 1/8, 2/8, 3/8, 4/8, 5/8, 6/8, 7/8) is stable enough to be utilized in the cathode materials. The PDOS of $Li_2Fe_{0.5}Co_{0.5}PO_4F$ shows both Co-3*d* and Fe-3*d* states contributing to the electronic states around the Fermi level, indicating it may possess better electronic conductivity than the *Pnma*-Li_2FePO_4F.

Acknowledgements

Financial support by the NSFC (21173037 and 21274017) is gratefully acknowledged.

Notes and references

[a] *National Engineering Laboratory for Power Battery (Jilin),Faculty of Chemistry, Northeast Normal University, Changchun 130024, China. E-mail: jpzhang@nenu.edu.cn*
[b] *Department of Material Science and Engineering, KTH--Royal Institute of Technology,SE-100 44 Stockholm,Sweden. Department of Physics and Astronomy, Division of Material Theory, Uppsala University*
† Electronic Supplementary Information (ESI) available: [(S1) The total DOS of Li_2FePO_4F and $LiFePO_4F$ (S2) The stability of $Li_2Fe_{1-x}M_xPO_4F$ (M = Co, Mn) (S3) Positions of Fe in *Pnma-Li_2FePO_4F* (S4) Volume changes of $Li_2Fe_{1-x}Co_xPO_4F$ upon delithiation (S5) Migration barriers for diffusion of Li atom in $Li_2Fe_{1-x}Co_xPO_4F$ (S6) The electron localization function (ELF) of $Li_2Fe_{1-x}Co_xPO_4F$ (x = 0.25, 0.5, 0.75)] See DOI: 10.1039/b000000x/
‡ Footnotes should appear here. These might include comments relevant to but not central to the matter under discussion, limited experimental and spectral data, and crystallographic data.

1. S. Megahed and B. Scrosati, *Journal of Power Sources*, 1994, **51**, 79-104.
2. J. M. Tarascon and M. Armand, *Nature*, 2001, **414**, 359-367.
3. M. Armand and J. M. Tarascon, *Nature*, 2008, **451**, 652-657.
4. H. Gwon, J. Hong, H. Kim, D. H. Seo, S. Jeon and K. Kang, *Energy & Environmental Science*, 2014, **7**, 538-551.
5. J. R. Croy, A. Abouimrane and Z. Zhang, *MRS Bulletin*, 2014, **39**, 407-415.
6. K. Amine, R. Kanno and Y. Tzeng, *MRS Bulletin*, 2014, **39**, 395-401.
7. A. K. Padhi, K. S. Nanjundaswamy and J. B. Goodenough, *Journal of The Electrochemical Society*, 1997, **144**, 1188-1194.
8. J. K. Ngala, S. Alia, A. Dobley, V. M. B. Crisostomo and S. L. Suib, *Chemistry of Materials*, 2006, **19**, 229-234.
9. F. Cheng, J. Liang, Z. Tao and J. Chen, *Advanced Materials*, 2011, **23**, 1695-1715.
10. A. S. Andersson, B. Kalska, L. Häggström and J. O. Thomas, *Solid State Ionics*, 2000, **130**, 41-52.
11. M. Gaberscek, R. Dominko and J. Jamnik, *Electrochemistry Communications*, 2007, **9**, 2778-2783.
12. S.-Y. Chung, J. T. Bloking and Y.-M. Chiang, *Nat Mater*, 2002, **1**, 123-128.
13. P. S. Herle, B. Ellis, N. Coombs and L. F. Nazar, *Nat Mater*, 2004, **3**, 147-152.
14. Z. Gong and Y. Yang, *Energy & Environmental Science*, 2011, **4**, 3223-3242.
15. S. H. Swafford and E. M. Holt, *Solid State Sciences*, 2002, **4**, 807-812.
16. S.-W. Kim, D.-H. Seo, H. Kim, K.-Y. Park and K. Kang, *Physical Chemistry Chemical Physics*, 2012, **14**, 3299-3303.
17. B. L. Ellis, W. R. M. Makahnouk, Y. Makimura, K. Toghill and L. F. Nazar, *Nature Materials*, 2007, **6**, 749-753.
18. M. Dutreilh, C. Chevalier, M. El-Ghozzi, D. Avignant and J. M. Montel, *Journal of Solid State Chemistry*, 1999, **142**, 1-5.
19. S. Okada, M. Ueno, Y. Uebou and J.-i. Yamaki, *Journal of Power Sources*, 2005, **146**, 565-569.
20. B. L. Ellis, T. N. Ramesh, W. N. Rowan-Weetaluktuk, D. H. Ryan and L. F. Nazar, *Journal of Materials Chemistry*, 2012, **22**, 4759.
21. N. R. Khasanova, O. A. Drozhzhin, D. A. Storozhilova, C. Delmas and E. V. Antipov, *Chemistry of Materials*, 2012, **24**, 4271-4273.
22. B. L. Ellis, W. R. M. Makahnouk, W. N. Rowan-Weetaluktuk, D. H. Ryan and L. F. Nazar, *Chemistry of Materials*, 2009, **22**, 1059-1070.
23. N. Recham, J.-N. Chotard, L. Dupont, K. Djellab, M. Armand and J.-M. Tarascon, *Journal of The Electrochemical Society*, 2009, **156**, A993-A999.

24. T. N. Ramesh, K. T. Lee, B. L. Ellis and L. F. Nazar, *Electrochemical and Solid-State Letters*, 2010, **13**, A43-A47.
25. M. M. Kalantarian, S. Asgari, D. Capsoni and P. Mustarelli, *Physical Chemistry Chemical Physics*, 2013, **15**, 8035-8041.
26. G. Hautier, A. Jain, T. Mueller, C. Moore, S. P. Ong and G. Ceder, *Chemistry of Materials*, 2013, **25**, 2064-2074.
27. S.-K. Hu, T.-C. Chou, B.-J. Hwang and G. Ceder, *Journal of Power Sources*, 2006, **160**, 1287-1293.
28. Z. Wang, S. Sun, D. Xia, W. Chu, S. Zhang and Z. Wu, *The Journal of Physical Chemistry C*, 2008, **112**, 17450-17455.
29. S. Luo, Y. Tian, H. Li, K. Shi, Z. Tang and Z. Zhang, *Journal of Rare Earths*, 2010, **28**, 439-442.
30. S. Shi, D.-s. Wang, S. Meng, L. Chen and X. Huang, *Physical Review B*, 2003, **67**, 115130.
31. D.-H. Seo, H. Gwon, S.-W. Kim, J. Kim and K. Kang, *Chemistry of Materials*, 2009, **22**, 518-523.
32. G. Kresse and J. Furthmüller, *Physical Review B*, 1996, **54**, 11169-11186.
33. G. Kresse and J. Furthmüller, *Computational Materials Science*, 1996, **6**, 15-50.
34. G. Kresse and J. Hafner, *Physical Review B*, 1993, **47**, 558-561.
35. G. Kresse and J. Hafner, *Physical Review B*, 1994, **49**, 14251-14269.
36. G. Kresse and D. Joubert, *Physical Review B*, 1999, **59**, 1758-1775.
37. K. Kang, C.-H. Chen, B. J. Hwang and G. Ceder, *Chemistry of Materials*, 2004, **16**, 2685-2690.
38. F. Zhou, M. Cococcioni, C. A. Marianetti, D. Morgan and G. Ceder, *Physical Review B*, 2004, **70**, 235121.
39. J. Bréger, Y. S. Meng, Y. Hinuma, S. Kumar, K. Kang, Y. Shao-Horn, G. Ceder and C. P. Grey, *Chemistry of Materials*, 2006, **18**, 4768-4781.
40. J. L. F. Da Silva, M. V. Ganduglia-Pirovano, J. Sauer, V. Bayer and G. Kresse, *Physical Review B*, 2007, **75**, 045121.
41. J. Yu, K. M. Rosso, J.-G. Zhang and J. Liu, *Journal of Materials Chemistry*, 2011, **21**, 12054-12058.
42. A. Jain, G. Hautier, C. J. Moore, S. Ping Ong, C. C. Fischer, T. Mueller, K. A. Persson and G. Ceder, *Computational Materials Science*, 2011, **50**, 2295-2310.
43. T. Mueller, G. Hautier, A. Jain and G. Ceder, *Chemistry of Materials*, 2011, **23**, 3854-3862.
44. G. Henkelman, B. P. Uberuaga and H. Jónsson, *The Journal of Chemical Physics*, 2000, **113**, 9901-9904.
45. M. K. Aydinol, A. F. Kohan and G. Ceder, *Journal of Power Sources*, 1997, **68**, 664-668.
46. M. K. Aydinol, A. F. Kohan, G. Ceder, K. Cho and J. Joannopoulos, *Physical Review B*, 1997, **56**, 1354-1365.
47. M. Ramzan, S. Lebègue and R. Ahuja, *Applied Physics Letters*, 2009, **94**, 151904.
48. E. Dumont-Botto, C. Bourbon, S. Patoux, P. Rozier and M. Dolle, *Journal of Power Sources*, 2011, **196**, 2274-2278.
49. X. Wu, Z. Gong, S. Tan and Y. Yang, *Journal of Power Sources*, 2012, **220**, 122-129.
50. X. Wu, J. Zheng, Z. Gong and Y. Yang, *Journal of Materials Chemistry*, 2011, **21**, 18630.
51. R. D. Shannon, *Acta Crystallographica Section A*, 1976, **32**, 751-767.